Methods in Ecology and Evolution | BRITISH ECOLOGICAL SOCIETY

RESEARCH ARTICLE

AngleCam: Predicting the temporal variation of leaf angle distributions from image series with deep learning

Teja Kattenborn[1,2] | Ronny Richter[2,3] | Claudia Guimarães-Steinicke[1,2] |
Hannes Feilhauer[1,2] | Christian Wirth[2,3]

[1]Remote Sensing Centre for Earth System Research (RSC4Earth), Leipzig University, Leipzig, Germany

[2]German Centre for Integrative Biodiversity Research (iDiv), Halle-Jena-Leipzig, Germany

[3]Systematic Botany and Functional Biodiversity, Institute of Biology, Leipzig University, Leipzig, Germany

Correspondence
Teja Kattenborn
Email: teja.kattenborn@uni-leipzig.de

Abstract

1. Vertical leaf angles and their variation through time are directly related to several ecophysiological processes and properties. However, there is no efficient method for tracking leaf angles of plant canopies under field conditions.

2. Here, we present AngleCam, a deep learning-based approach to predict leaf angle distributions from horizontal photographs acquired with low-cost time-lapse cameras. AngleCam is based on pattern recognition with convolutional neural networks and trained with leaf angle distributions obtained from visual interpretation of more than 2500 plant photographs across different species and scene conditions.

3. Leaf angle predictions were evaluated over a wide range of species and scene conditions using independent samples from visual interpretation ($R^2 = 0.84$) and compared to leaf angle estimates obtained from terrestrial laser scanning ($R^2 = 0.75$). AngleCam was tested for the long-term monitoring of leaf angles for two broadleaf tree species in a temperate forest. The plausibility of the predicted leaf angle time series was underlined by its close relationship with environmental variables related to transpiration.

4. The evaluations confirm that AngleCam is a robust and efficient method to track leaf angles under field conditions. The output of AngleCam is compatible with a range of applications, including functional-structural plant modelling, Earth system modelling or radiative transfer modelling of plant canopies. AngleCam may also be used to predict leaf angle distributions for existing data, for instance from PhenoCam networks citizen science projects.

KEYWORDS
convolutional neural networks, ecophysiology, leaf angles, leaf inclination, leaf tilt, plant movement, time series

1 | INTRODUCTION

Plants show a diverse configuration of leaf angles across species and growth forms. Already Darwin and Darwin (1880) noted that the configuration of a plant's leaf angles varies in diurnal rhythms, changes through phenology and reacts on environmental stimuli, such as light availability, temperature, competition or water availability. This can include nastic movements, that is, non-directional movements to stimuli such as irradiance or temperature, tropisms which are directed to a stimulus (e.g. the course of the sun), adhesion of precipitation, active and passive responses to drought and heat stress such as drooping or wilting of leaves (Apelt et al., 2017; Niinemets, 2010; Puglielli et al., 2017). Such imprints of environmental stimuli on leaf angular orientations differ considerably between growth forms, species and even genotypes (Geldhof et al., 2021).

The orientation of individual leaves in a canopy can be described by their vertical surface angles (0° horizontal and 90° vertical). The statistical distribution of vertical leaf angles within a canopy is described as leaf angle distributions. Information on leaf angles is relevant for various fields. Leaf angles have direct influence on the light interception and photon yield of plants (Mantilla-Perez & Salas Fernandez, 2017; Pepper et al., 1977; Rogers et al., 2017; Sarlikioti et al., 2011). Leaf angles may not only determine productivity, but are also an important trait studied in community ecology to understand competitive abilities of plants (Hikosaka & Hirose, 1997; Kattenborn et al., 2019; Mullen et al., 2006; Niinemets, 2010). Changes in leaf angles are a direct indicator of stresses, such as excess radiation, heat and drought stress (Ehleringer & Comstock, 1987; Geldhof et al., 2021; Van Zanten et al., 2010), which, in turn, can strongly alter the energy balance of canopies (Leuzinger & Körner, 2007; Sastry et al., 2018). The interplay of leaf angles with incoming radiation also greatly affects scattering processes of plants across wavelengths (Berger et al., 2018; Jacquemoud et al., 2009; Kattenborn et al., 2018) and, hence, have a large effect on reflectance and fluorescence signals in Earth observation data (Braghiere et al., 2021; Dechant et al., 2020; Hase et al., 2022; Xu et al., 2021).

Despite the importance of leaf angles for a series of applications, there is no efficient and automated method to track the temporal variation of leaf angles or their distribution in plant canopies under field conditions (Berger et al., 2018; Niinemets, 2010). Inertial measurement units (IMU) attached to single leaves proved to be an effective approach to track movements of individual leaves (Geldhof et al., 2021), but this is not scalable to track leaf angle distributions in whole plant canopies. Methods based on 3D point clouds derived from photogrammetry (Qi et al., 2019) or terrestrial laser scanning (TLS; Itakura & Hosoi, 2019; Stovall et al., 2021) enable the estimation of leaf angle distributions, but require either expensive equipment, sophisticated data acquisition and processing procedures, and are, hence, hardly scalable for tracking variations at high temporal resolutions (e.g. <hourly) and long time periods.

Stereo imaging techniques with rigs of conventional cameras and image matching or depth analysis were shown to be effective for multitemporal analysis (Bernotas et al., 2019; Biskup et al., 2007; Müller-Linow et al., 2015). However, such approaches require sophisticated hardware configurations and calibration as well as image acquisition in nadir view, which is often hard to realize for various applications and field conditions. Simpler and low-cost methods based on conventional cameras were presented by Pisek et al. (2011) and Zou et al. (2014), where angles of leaves that are perpendicular to the camera orientation are estimated from the imagery by a human interpreter. This approach was successfully applied across different plant species and times steps (Hase et al., 2022; Kattenborn et al., 2018), but lacks automation and, thus, efficiency (but see Raju et al., 2020, for a semi-automatic approach). However, with advances in computer vision-based pattern recognition and deep learning (Kattenborn et al., 2021; Mohanty et al., 2016; Singh et al., 2018), such interpretation tasks may be taken over by an artificial intelligence.

The currently most prominent deep learning technique for predictive image analysis is convolutional neural networks (CNNs), which learn the image features that are required to predict the target property (Albawi et al., 2017). In the recent years, a series of studies successfully applied CNN for predicting vegetation properties from conventional RGB cameras (Cao & Xin, 2021; Correia et al., 2020; Schiefer et al., 2020; Schiller et al., 2021). Depending on the model complexity, the training process of such models may be time-consuming, but the prediction task of a trained model is extremely fast (Kattenborn et al., 2021). In concert with increasing performance of outdoor-capable cameras (timelapse cameras or PhenoCams), such deep learning-based method may prove to be an effective method to track temporal variation in leaf angles.

Here, we present and evaluate AngleCam—a method to estimate leaf angle distributions from plant images and deep learning-based pattern recognition techniques. First, we evaluated AngleCam for different and complex leaf forms of different plant species using independent samples as well as leaf angle estimates from TLS. Second, we test AngleCam under field conditions for long-term monitoring of leaf angle distribution at high temporal resolution (3 min) over long time periods (4 months). For this, we attached 19 cameras to four individuals of two tree species with contrasting leaf forms and functioning at the Canopy Crane research platform (Leipzig Canopy Crane [LCC]) of the German Centre for Integrative Biodiversity Research (iDiv) Halle-Jena-Leipzig. The plausibility of these time series was additionally assessed by testing their correspondence with environmental drivers monitored on-site.

2 | METHODS

The methods comprise the acquisitions of RGB images using timelapse cameras, the generation of reference data with visual interpretation, the design and training of the CNN model (AngleCam), its independent evaluation using leaf angle estimates from TLS and the model application to image time series.

FIGURE 1 Illustration of the leaf angle definition and the leaf surface normal, that is, the perpendicular vector to the tangential plane at the surface (left), the positioning of cameras mounted in trees at the LCC site (centre), and an example of a camera (Brinno TLC-200 Pro) installed within a crown (right)
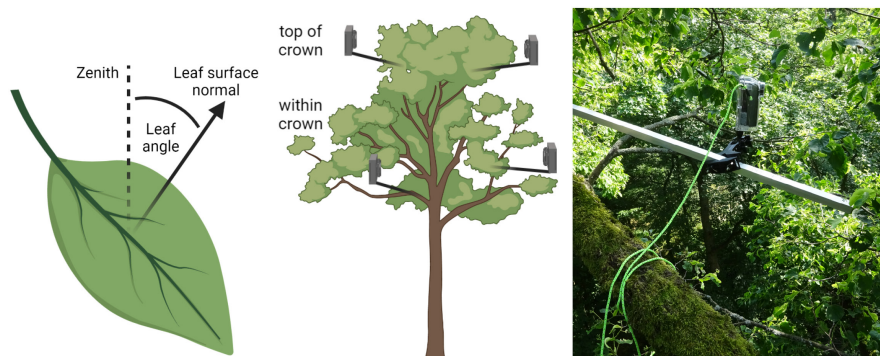
2.1 | RGB image acquisition

All images in this study were acquired with TLC-200 Pro timelapse cameras (Brinno, The Netherlands). The TLC-200 Pro records time-lapse videos with a resolution of 1280×690 pixels in high dynamic range (HDR) mode. The HDR mode is particularly beneficial for scenes with complex illumination conditions, as is often the case in vegetation canopies. The TLC-200 Pro can be operated autonomously with batteries and SD card-based flash memory. The time-lapse videos can be readily converted to single image frames (see provided code). Therefore, in the following, when the capturing of images is described, the capturing of videos and subsequent conversion to single images is meant. All imagery in this study was acquired with a horizontal camera orientation (visually estimated).

As detailed below, using the TLC-200 Pro, we generated three image datasets with reference data, including

1. a heterogeneous dataset recorded in the area of Leipzig to facilitate the model transferability,
2. Image time series recorded at the LCC to test the temporal tracking of leaf angles and
3. in addition to the two before-mentioned datasets, which were used for model training, another dataset was acquired together with terrestrial laser scans in the Botanical Garden of Leipzig University for independent model evaluation (described in Section 2.4).

The first dataset acquired in the area of Leipzig was generated in 2021 and included various settings and locations to facilitate the transferability of a CNN model across scene characteristics and plant species. This imagery was acquired in natural and semi-natural sites, parks, from indoor plants and gardens. This resulted in a dataset of approximately 60 different species, mostly belonging to herbs, shrubs and deciduous tree species. The camera was operated by hand and for each plant a series of pictures was generated from varying azimuth angles and distances (<2 m). From these acquisitions, finally 580 images were selected for model training and validation (Section 2.2).

The dataset on image time series was acquired in 2021 at the LCC site of the German Centre for Integrative Biodiversity Research (iDiv) Halle-Jena-Leipzig. The crane is located in the Leipzig floodplain forest, a structurally complex hardwood forest. The dominant tree species are European ash (*Fraxinus excelsior* L.), English oak (*Quercus robur* L.), Sycamore maple (*Acer pseudoplatanus* L.), European hornbeam (*Carpinus betulus* L.) and small-leaved lime (*Tilia cordata* Mill) (see Richter et al., 2021, for details). The resulting images were also used for model training and evaluation (Section 2.2) and to test the long-term monitoring of leaf angles (Section 2.5). For image acquisition, the cameras were permanently mounted in tree crowns of four mature trees of *A. pseudoplatanus* and *T. cordata* (two individuals per species). To mount and service the cameras at the tree crowns, we used the gondola of the canopy crane, which enabled us to directly access individual trees at different heights. The cameras were fixed to aluminium poles (2 cm diameter, 2 m length), which, in turn, were fixed to robust branches of the target trees. The cameras were protected with water-resistant housings available from the manufacturer. In total, we attached 19 cameras. Given that leaf angles are known to vary considerably along the vertical gradient of plant canopies (Niinemets, 2010), we attached the cameras at two relative height levels: For each tree, at least two cameras were mounted at the crown top (approximately 30 m height) and two cameras within the canopy (approximately 20 m height) (Figure 1).

The cameras attached to the trees were set to a 1 min interval and the acquisition period was limited to 08:00–20:00 CEST to constrain data loads and battery consumption. The data acquisition period ranged from the beginning of June to the end of September 2021. In this period, the cameras were serviced two times, which included the exchange of batteries, exchange of SD cards, cleaning of lenses from pollen and dust and adjusting potential changes in camera orientations (the site was subject to multiple storm events during 2021). A sample of 2190 images acquired at the canopy crane facility was included in the model training and validation (Section 2.2). These image samples were selected manually to cover diurnal cycles and different weather conditions.

The acquisition date and time of each frame was automatically documented with a timestamp at the bottom of each image (an area expanding from left to right with 30 pixels height). These timestamps were removed from the imagery and the date and time were extracted to text files using the optical character recognition engine *tesseract* (R-package TESSERACT, vers. 4.1), which utilizes deep learning-based long short-term memory networks.

A gap-less image acquisition was not possible for all mounted cameras. Some data gaps were caused by multiple heavy storms that took place in 2021 in Leipzig that bent the suspension or at least changed the orientation of the cameras so that the imagery was not usable. In one case, a full time series was not recorded due to incorrect operation and in another case the camera was defect.

2.2 | Generation of training and validation data

Training deep learning-based pattern recognition often requires large quantities of training data. To effectively generate a large number of samples, we used visual interpretation of the RGB imagery. Previous studies proposed to estimate leaf angle distributions from leaves that are perpendicular to the line of sight in horizontal images by digitally measuring the angle (0–90°) between the zenith and an estimated leaf surface normal (Pisek et al., 2011; Ryu et al., 2010). Thereby, the leaf surface normal is defined as perpendicular vector to the tangential plane at the surface (Figure 1). Such techniques have been successfully applied in a range of studies (Hase et al., 2022; Kattenborn et al., 2018; Xu et al., 2021). However, this approach is only applicable for leaves that are perpendicular to the line of sight of the image, which can, hence, greatly limit the amount of samples per image. Furthermore, an explicit leaf surface normal cannot be directly delineated for complex leaf forms, such as found for several species (including *A. pseudoplatanus* studied here) or at certain plant states, for example, leaf rolling or drooping (Ryu et al., 2010). To pragmatically overcome these limitations, we visually estimated the mean surface angle of whole leaves (0–90°), assuming that the human visual cortex can sufficiently infer the geometrical orientation of leaf surfaces from horizontal images (Kim & Burge, 2020; Spelke et al., 2010). Thereby, inaccuracies are expected, but as long as the latter are normally distributed and the dataset is large enough, they can be compensated by machine learning algorithms (Kattenborn et al., 2021; Rolnick et al., 2017).

We created a R-based pipeline (R Core Team, 2013) that displays images and enables the interpreter to select individual leaves by clicking and subsequently enter the estimated leaf angle. As suitable trade-off between sampling speed and robustness, we estimated leaf angles for 20 samples for each image. To obtain a representative sample for a given image, evenly distributed points were overlaid on the image during visual interpretation, from which the closest leaf was selected for interpretation. Based on the image samples selected in Section 2.1, reference data were generated for a total of 2770 images, including 580 images obtained at various sites around Leipzig and 2190 images from the LCC site.

2.3 | CNN model training

Considering that 20 leaf angle samples per image may be too sparse to robustly represent an actual leaf angle distribution, we trained the CNN model with probability distributions derived from these samples. The probability distributions were estimated using the two-parameter beta distribution function, which was found to accurately describe the probability density of a leaf angles in plant canopies (Goel & Strebel, 1984; Wang et al., 2007). The parameters of the beta distribution (α, β) were fitted using the maximum likelihood estimation (mle, R-package FITDIST, v.1.1-5).

We did not train the CNN model on explicitly predicting the fitted beta distribution parameters (α, β), assuming that in certain conditions the actual leaf inclination distribution may depart from such an idealized beta distribution. Instead, the model was trained to predict a probability density from 0 to 90° at 2° intervals derived from the fitted beta distribution. For model regularization, we augmented the leaf angle distributions of the training data (Schiller et al., 2021) based on the standard deviation of the beta distribution parameters (α, β) obtained from the mle fit. For each image in the training sample, 50 variants of leaf angle distributions were generated by randomly sampling α and β parameters within 20% of the estimated standard deviation. During the training process, which repeatedly iterates over all training images in multiple epochs (details below), one of these 50 variants was randomly selected as reference. The model validation was performed with the leaf angle distribution as obtained from the initial mle fit.

The CNN model was implemented in R using the Keras and TensorFlow frameworks (vers. 2.9.1). The imagery was pre-processed on the fly using a TensorFlow input pipeline and included the conversion from integer (0–255) to floating values (0–1) and cropping the imagery to 512×512 pixels. A resolution of 512×512 was selected as being an ideal compromise between model accuracy and efficiency during initial tests. For training data augmentation, the imagery was cropped to 512×512 pixels using a random location within the 1280×690 pixels. Yet, we constrained the cropping locations not to overlap with the image boarders, defined as the outermost 10% of the original imagery. The imagery used for validation and prediction was cropped to 512×512 pixels along the shortest edge of the input imagery while maintaining the original aspect ratio.

As CNN feature extractor, we used EfficientNet-B7 (Tan & Le, 2019), which is at the time of writing reported to be one of the most accurate and efficient backbones (Hoeser & Kuenzer, 2020). The backbone was initialized with random weights and a drop connect rate of 0.2. The EfficientNet-B7 backbone was followed by a global average pooling and a dense layer with 43 units, corresponding to the 2° interval between 0 and 90° of the leaf angle distribution (Figure 2). The resulting model was trained with 200 epochs and a batch size was 10. We choose the adam optimizer with a learning rate of 0.0001. Of the 2770 training samples, 2570 were used for training and 200 were used to monitor the training process (onward validation holdout; sample numbers were set arbitrarily). The final model was selected based on the lowest loss (mean squared error) obtained from the validation data and evaluated with independent estimates of leaf angle distributions obtained from TLS scanning (Section 2.4).
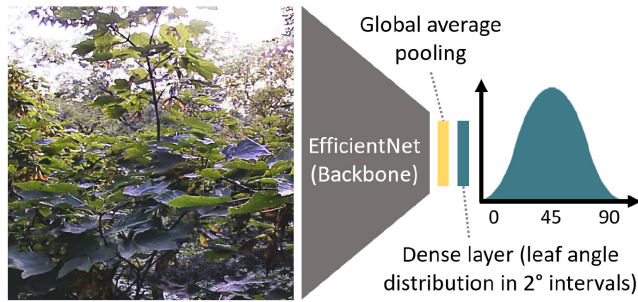
FIGURE 2 The AngleCam model structure used in this study to predict a leaf angle distribution from a single image. The basis for the latter is the EfficientNet-B7 backbone, followed by a global average pooling and a dense layer. The dense layer results in a vector of length 43 representing the leaf angle distribution at a 2° interval

2.4 | CNN model evaluation with TLS

The CNN model evaluation using validation holdouts (Section 2.3) tests the model's ability to reproduce the reference data obtained from visual interpretation, but cannot inform on whether the predicted leaf angles (or the results obtained from visual interpretation) are actually accurate. Therefore, we evaluated the model performance for predicting leaf angle distributions with TLS-based estimates, which provide an entirely independent comparison. Moreover, TLS-based estimates are assumed to enable the most robust estimation of leaf angle distributions (Stovall et al., 2021; Vicari et al., 2019). We predicted leaf angle distributions from the TLS scans using the TLSLeAF method (Stovall et al., 2021). TLSLeAF was successfully validated with indoor experiments and real-world data of different forest types, including loblolly pine, hemlock, broadleaf, tropical broadleaf and mangrove forests (Stovall et al., 2021). TLSLeAF estimates leaf angles from surface normals estimated from multiple laser returns of a leaf. For this, the algorithm first estimates surface normals (Bailey & Mahaffee, 2017) and separates leaf and woody components using a random forest model and spatial eigenvectors derived from surface normals estimated at multiple scales (Moorthy et al., 2019).

As test dataset we acquired image and TLS data for 25 species of different growth and leaf forms in the Botanical Garden of Leipzig University, Germany. The sampled species included *Adiantum capillus-veneris* L., *Anthurium amnicola* Dressler, *Bixa orellana* L., *Bonellia macrocarpa* Cav., *Calathea wiotii* Petersen, *Caliphruria subedentata* Baker, *Carica papaya* L., *Capparis ferruginea* L., *Deherainia smaragdina* Decne., *Dorstenia contrajerva* L., *Fittonia albivenis* Lindl. ex Veitch, *Heliconia stricta* Huber, *Pachystachys lutea* Nees, *Oplismenus hirtellus* L., *Pilea densiflora* Kunth, *Pseuderanthemum alatum* Nees, *Pitcairnia imbricata* Brongniart, *Pteris tremula* R. Br., *Rhytidophyllum tomentosum* (L.) Mart., *Tillandsia cyanea* Linden ex K. Koch, *Tradescantia spec*. and *Vriesea ospinae* H. Luther. We generated two TLS scans using a Faro Focus 3D X330 (FARO Technologies Inc., 2019). The scans included RGB colour information obtained from the internal cameras of the scanner. Considering the results of Stovall

et al. (2021), we positioned the scanner at a maximum distance of 5 m to the target plants. Afterwards, the target species were imaged with the Brinno TLC-200 Pro from multiple positions with horizontal orientation. Depending on the image quality, 15–26 images per plant species were used for predicting the leaf angle distributions with the trained AngleCam models and subsequently averaged (these images were not included in the training process of AngleCam).

The raw TLS scans were exported as gridded point clouds in .ptx format using the proprietary software 'Scene' (version 5.2.0, Faro Technologies, Inc.). We applied TLSLeAF with a spatial sub-sampling of the point cloud of 0.005 m, an upper limit of the scattering angle of 80° (angle between leaf surface normal and beam direction), spatial scales of the leaf-wood classifier of 0.1, 0.5, 0.75 and without topography correction. The result was a new point cloud with scalar values for each point representing the estimated leaf surface angles.

We cleaned the TLSLeAF outputs from noise and points that do not represent leaves (e.g. twigs, ground). For this, we applied statistical outlier removal on the raw point clouds (CloudCompare, 2022) and manually clipped the raw point clouds to individual segments for each species. Using the RGB information and the structure of the point cloud, we cleaned the individual point clouds so that only leaves remained. Using a minimum distance threshold of 0.005 m, the cleaned subsets of the raw point clouds were then used to extract a clean version of the TLSLeAF output for each individual species. The point-based leaf angle estimates of these TLSLeAf subsets were then aggregated to leaf angle distributions as defined in the AngleCam workflow (binned frequencies between 0 and 90° at 2° intervals). Additional comparisons between the AngleCam and the TLSLeaf output were performed based on average leaf angles derived from the leaf angle distributions.

2.5 | CNN model application to image time series

The AngleCam model obtained in Section 2.2 was applied to the individual image time series generated from the 19 cameras mounted at the trees at LCC site. The time series were reduced to 3-min intervals totalling to 317,348 images. To simplify the evaluation and analysis of the predicted time series, the predicted leaf angle distributions were converted to average leaf angles.

The plausibility of the predicted leaf angle time series was further assessed by testing the strength of their relationship with time series of environmental variables measured at the top of the LCC. These included direct and diffuse solar radiance [W/m^2], rain [mm], rain duration [s/10 min], air temperature [°C], air pressure [hPa], relative humidity [%] and wind speed [m/s]. Additionally, soil humidity [m^3/mm] was included, which is measured at two positions of the site in 50 cm depth. All environmental variables were measured in 10-min intervals (see Richter et al., 2022, for further details on the instrumentation). The strength of the relationship was tested for the individual time series of each camera using predictive modelling, with leaf angle-related time series being the response (*y*) and environmental variables the predictors (*x*). For each observation of the

environmental variables (10-min interval), the closest observation of the respective leaf angle time series was matched (3-min interval). We generated separate models to predict both the moving mean (triangular moving mean) and the moving standard deviation of the predicted leaf angle time series (window size of 4h). We choose the random forest algorithm (Breiman, 2001) with the arbitrarily set parameters *ntree* = 500 and *mtry* = 3. To avoid optimistic model performance estimates induced by temporal autocorrelation, we split the time series into 10 equally spaced bins (1–10), where odd and even bins were used as training subset and validation subset, respectively. The validation subset was used to calculate the model accuracy (R^2) of each random forest model (separate models for moving mean and moving standard deviation and each camera).

To estimate the relative contribution of each predictor on the model accuracy, the mean variable importance (conditional permutation importance, Debeer et al., 2021; Strobl et al., 2008) for predicting the moving mean and the moving standard deviation, respectively, was derived from the random forest models. We normalized the variable importance (*Varimp*) to relative values [%] to ease the interpretation and comparison ($Varimp_i / \sum Varimp_{1-n} \times 100$).

3 | RESULTS

3.1 | Model evaluation using holdouts and TLS-based estimates

For simplicity, model performance was partly quantified using average leaf angles obtained from the leaf angle distributions. The first model performance evaluation was based on the reference data obtained by visual interpretation from the dataset acquired around Leipzig and at the LCC. The estimated model performance based on average leaf angles was similar between the training (R^2 of 0.93) and

validation samples ($R^2 = 0.84$) and no signs of overfitting or bias were observed (Figure 3a,b). The second model evaluation comparing average leaf angles obtained from the AngleCam and the TLSLeAF method showed a high linear correspondence ($R^2 = 0.75$) over the 25 plant species sampled at the Botanical Garden (Figure 3c). A linear model fit revealed a direct agreement between both estimates ($m = 0.97$) and a relative overestimation of the AngleCam method of 11.1 degree (c).

The predictions derived from AngleCam also showed a high agreement with TLSLeAF estimates when comparing the actual leaf angle distributions (see Figure 4). The normalized mean average error (NMAE) was 6.7% over the 25 species. The NMAE was stable over all species (SD = 1.5%).

3.2 | Evaluation of long-term time series

All time series follow a consistent course without apparent artefacts or unrealistic variations (see Figures 5 and 6 for two individual trees. Results for the other trees are given in the Appendix). Relatively smooth variations in average leaf angles can be observed over several days or even weeks. Similarly, variation in the daily range of average leaf angles can be observed over time. These temporal features show similarities between time series of multiple cameras as long as they both emerge from either within or top crown positions. Highest consistency of average leaf angles at the 3-min interval was observed for time series derived from cameras mounted within canopies (Pearson's $r = 0.32$) rather than on top of canopies (Pearson's $r = 0.16$). No apparent consistency was found between *A. pseudoplatanus* and *T. cordata* (Figures 5 and 6).

In addition to patterns observed over several days, the time series also exhibit diurnal patterns. Often and particularly for *T. cordata* during sunny days, an increase in average leaf angles until noon and a decline towards the evening was observed (Figure 6).
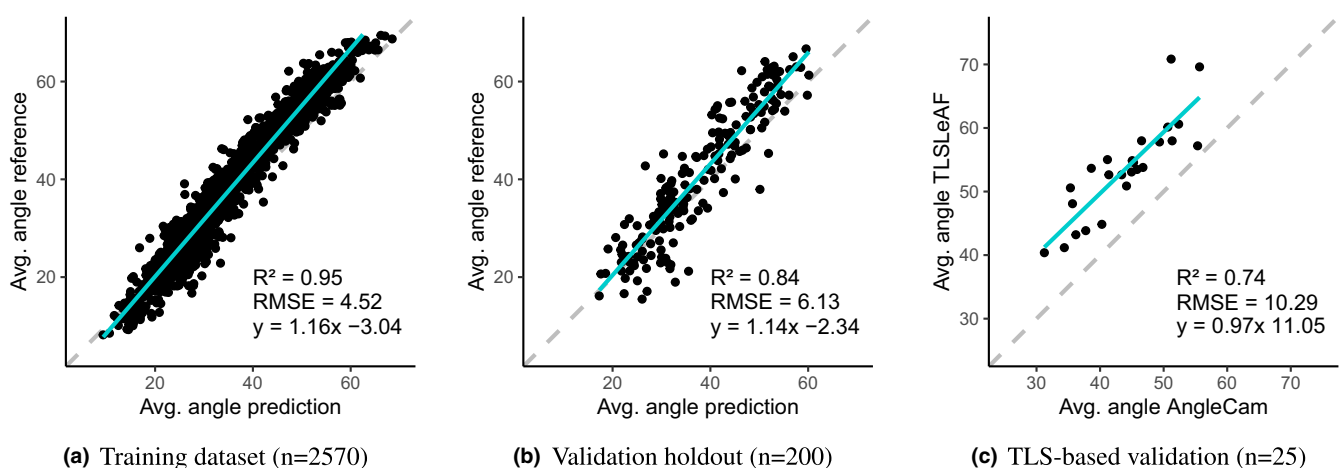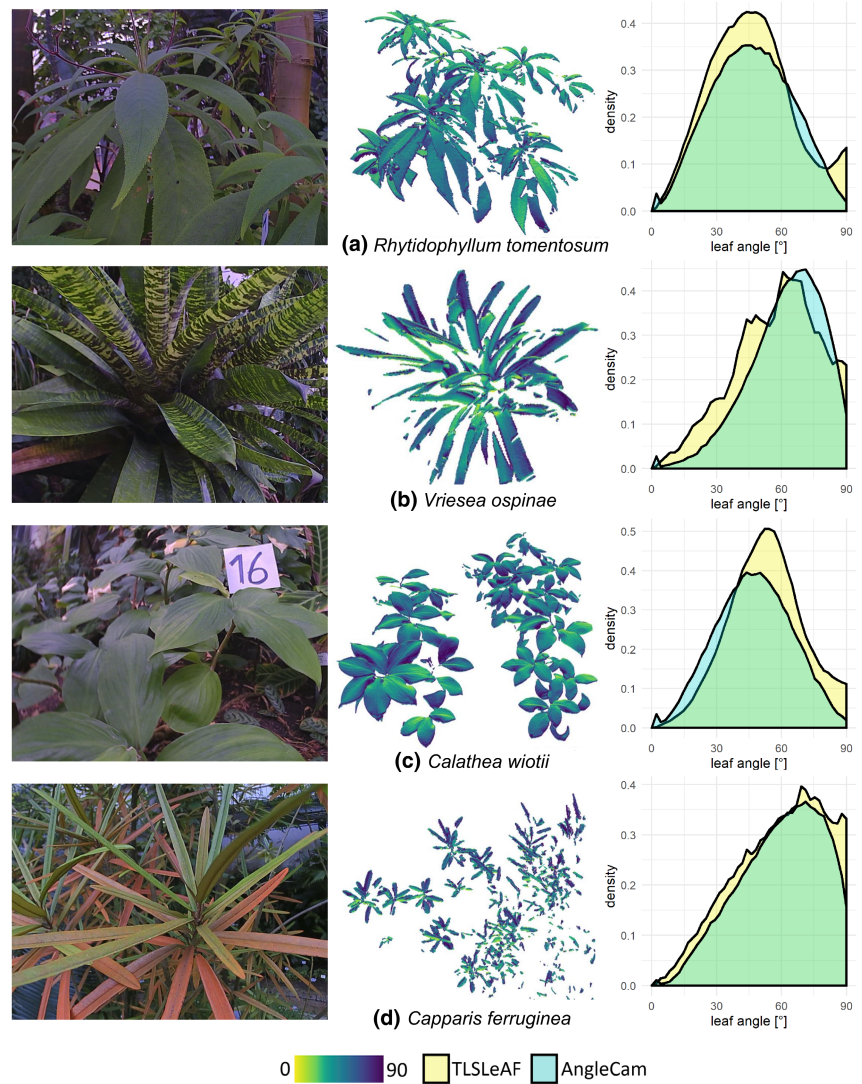

(a) Training dataset (n=2570) **(b)** Validation holdout (n=200) **(c)** TLS-based validation (n=25)

FIGURE 3 Model validation using the average leaf angle as calculated from leaf angle distributions: (a) and (b) show model predictions against the reference data from visual interpretation and (c) against leaf angle distributions obtained from the TLSLeAF pipeline. The reference data from visual interpretation (a, b) was obtained around Leipzig and the Leipzig Canopy Crane (LCC; total of 2770 images) and the TLS-based comparison (c) was based on a separate dataset of 25 species in the Botanical Garden Leipzig

FIGURE 4 Comparison of AngleCam- and TLSLeAF-derived leaf angle distributions for 4 out of 25 different species. Left: Example images used for predicting leaf angles using AngleCam. Centre: Point clouds coloured with leaf angle estimates derived from TLSLeAF (30° vertical viewing angle). Right: Comparison of the leaf angle density distributions. The AngleCam distributions show the raw prediction output, while the TLS-based distributions are derived from a plant-wise aggregation of the point cloud-based TLSLeAF output (centre)

(a) *Rhytidophyllum tomentosum*

(b) *Vriesea ospinae*

(c) *Calathea wiotii*

(d) *Capparis ferruginea*

0 ▮ 90   ▢ TLSLeAF   ▢ AngleCam

To be clear, the leaf surface angles do not inform if the leaves are pointing upward or downward (axis from leaf petiole to tip) but represent the integrated angle of the leaf surface. An increase in leaf angles can, hence, result from a downward tilt of the leaves. This was confirmed by visual inspection of individual frames and corresponding average leaf angle predictions. An example is shown in Figure 8, where leaves appear to move downwards from morning to noon (↑ average leaf angle), followed by an upward movement until evening (↓ average leaf angle).

For days with pronounced winds, cloudiness and precipitation, the temporal variation in leaf angles was observed to depart from the above-described diurnal patterns. For instance, a large variation in leaf angles and even short-term change in diurnal patterns could be observed following rain events, including the 22nd June, 8th July 23rd August (see Figure 7).

The correspondence of leaf angles with environmental drivers was unexpectedly high, further underlining the plausibility of the predicted time series. Predicting the moving mean of the average leaf angle using random forest models and environmental variables resulted in a R^2 of 0.985 for *A. pseudoplatanus* and 0.988 for *T.*

cordata. Similarly, the R^2 for the moving standard deviation was 0.976 and 0.977 for *A. pseudoplatanus* and *T. cordata*, respectively. Model performances were comparably high for time series corresponding to crown tops and within crowns, with R^2 of 0.986 and 0.988 for moving mean of average leaf angles at crown top and within crowns, respectively, and R^2 of 0.977 and 0.976 for the moving standard deviation of average leaf angles at crown tops and within crowns, respectively (see Appendix for details).

The relative variable importance of the environmental variables (the decrease in model accuracy when the variable is not included) indicated that soil humidity, air pressure, temperature and relative humidity were overall most important for the models (Figure 7). Lower importance was estimated for wind speed and solar radiation, while rain and rain duration had the lowest contribution. The variable importance changed considerably between the random forest models for the prediction of the moving mean and the moving standard deviation of leaf angles. For instance, wind speed and rain duration were considerably more important for predicting the variation of leaf angles over time (moving standard deviation; Var imp sd) compared to predicting the mean leaf angle over time (moving mean; var imp mean).
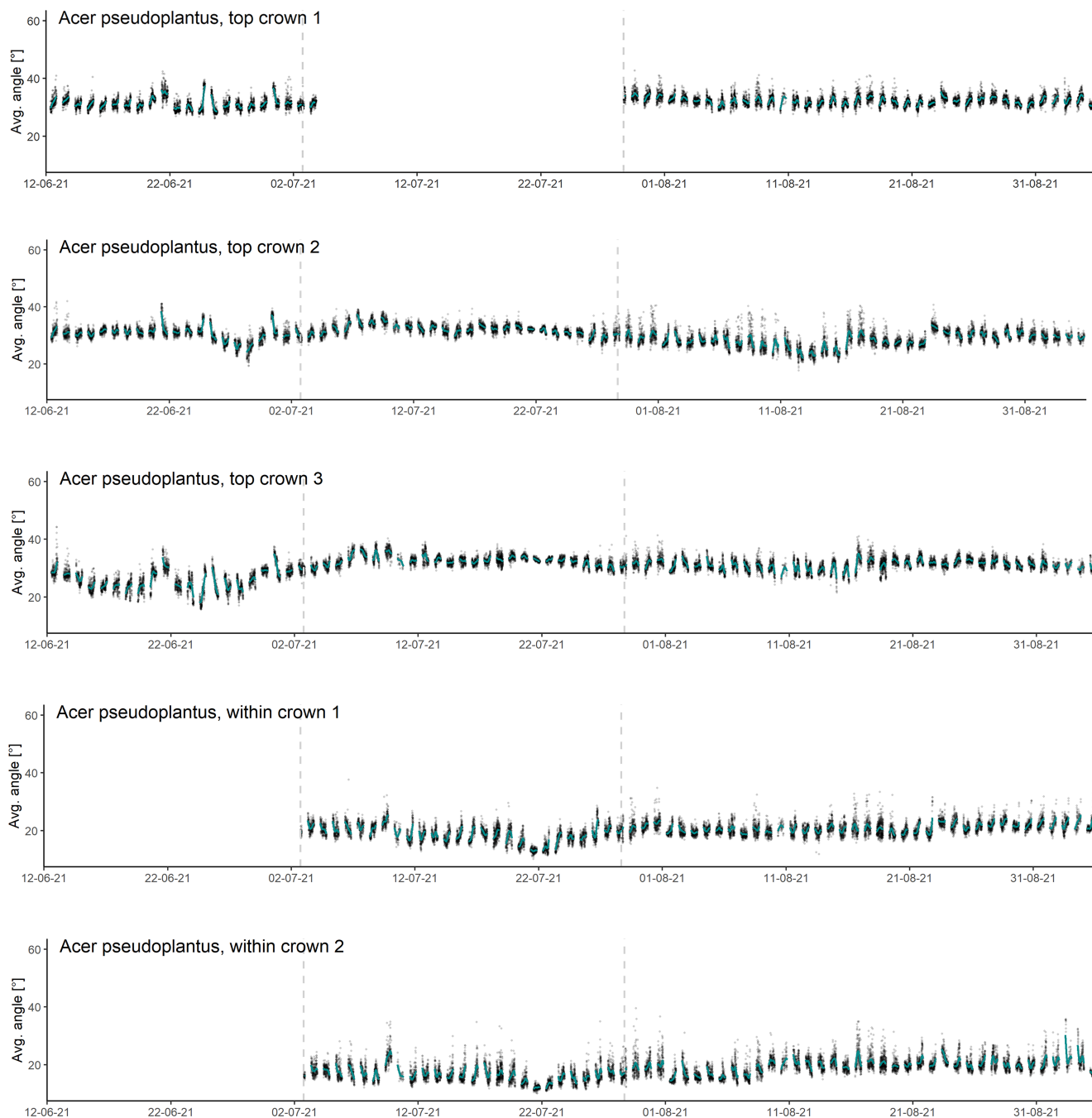
FIGURE 5 Time series of average leaf angles (derived from the predicted leaf angle distributions) from cameras on top and within the crown of tree 346 (*Acer pseudoplatanus*). Cyan lines indicate moving means (4 h). Vertical lines indicate dates at which the cameras were serviced

4 | DISCUSSION

4.1 | Model evaluation using holdouts and TLS-based estimates

Predictions of leaf angle distributions were evaluated with (i) validation holdouts of the reference data obtained by visual interpretation and (ii) leaf angle estimates derived from TLS. The visual interpretation enabled to evaluate the model performance

with a large sample over various species, growth forms and scene characteristics. Yet, this may not have revealed if a bias of leaf angle estimates was introduced from the visual interpretation itself. This was compensated by the TLS-based evaluation, which revealed a strong linear relationship of the AngleCam and the TLSLeAF method. The apparent systematic overprediction found for AngleCam method may result from the visual interpretation. However, the overprediction may also result from artefacts in the TLS scans observed at the edges of leaves (false-positive LiDAR
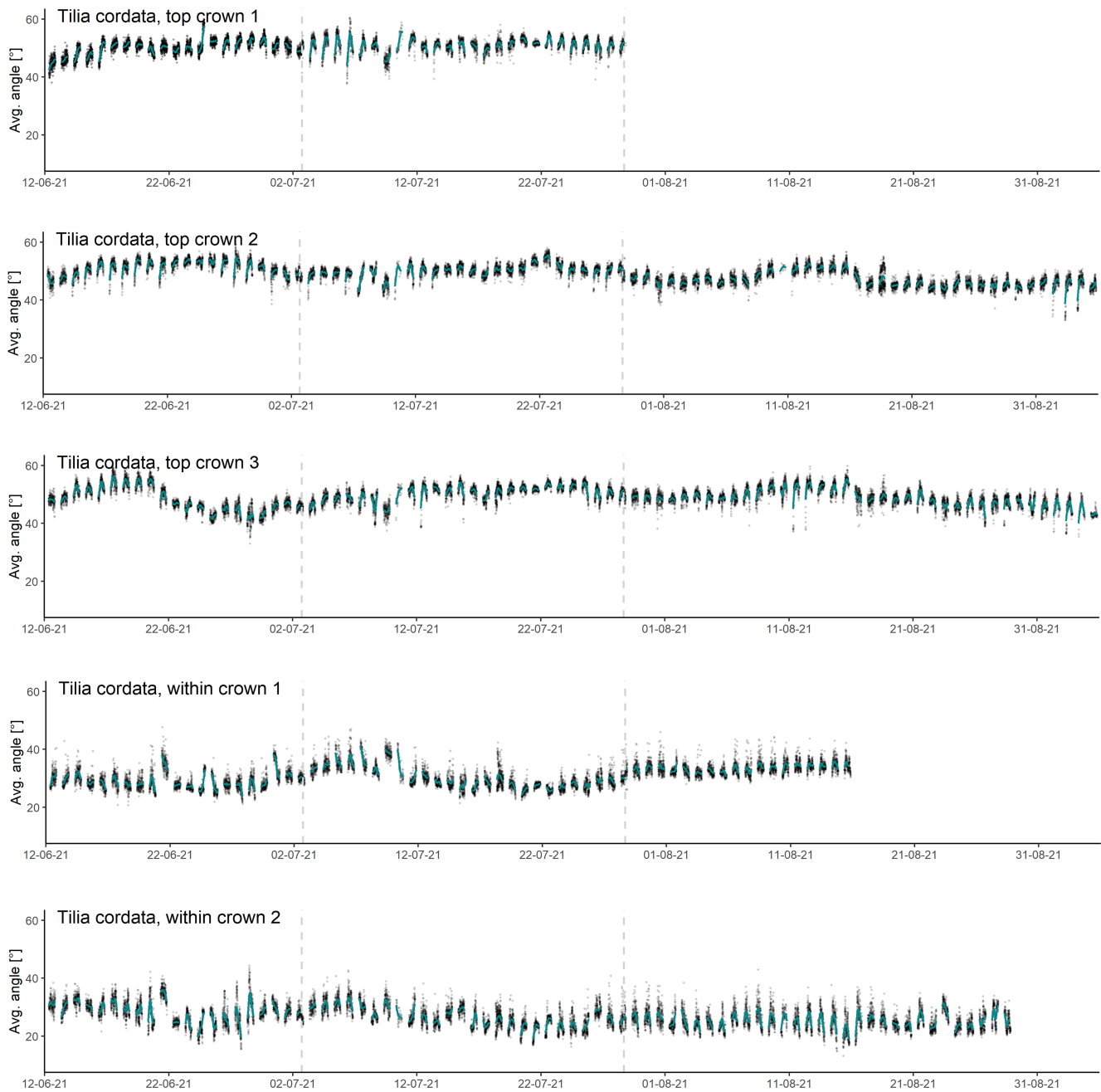
FIGURE 6 Time series of average leaf angles (derived from the predicted leaf angle distributions) from cameras on top and within the crown of tree 343 (*Tilia cordata*). Cyan lines indicate moving means (4 h). Vertical lines indicate dates at which the cameras were serviced

returns), for which predominantly high leaf angles were predicted with the TLSLeAF method. The point clouds were statistically filtered for noise and manually cleaned, but the latter was limited due to the data volumes and the structural complexity of most plant canopies. Based on the inspection of the TLSLeAF outputs, these artefacts (originating from scanning, not the analysis) may explain to a considerable extent systematically higher leaf angles obtained with the TLS-based method. Nevertheless, the comparison of TLSLeAF and AngleCam not only demonstrated a high accuracy and transferability of the latter, but also hints that robust leaf angle estimates can indeed be obtained from visual interpretation.

4.2 | Evaluation of long-term time series

The AngleCam method was successfully tested on image series derived from various camera positions of four tree individuals as indicated by the evaluation of holdouts (Figure 3), the visual inspection (Figure 8) and the correspondence with environmental drivers (Figure 7 and Appendix). The time series revealed temporal patterns on multiple scales. Diurnal patterns and oscillations were also observed by other studies, for example, Geldhof et al. (2021), who used IMU sensors attached to single leaves in an indoor experiment and found that such patterns can drastically change between species and environmental conditions. Here, the time series
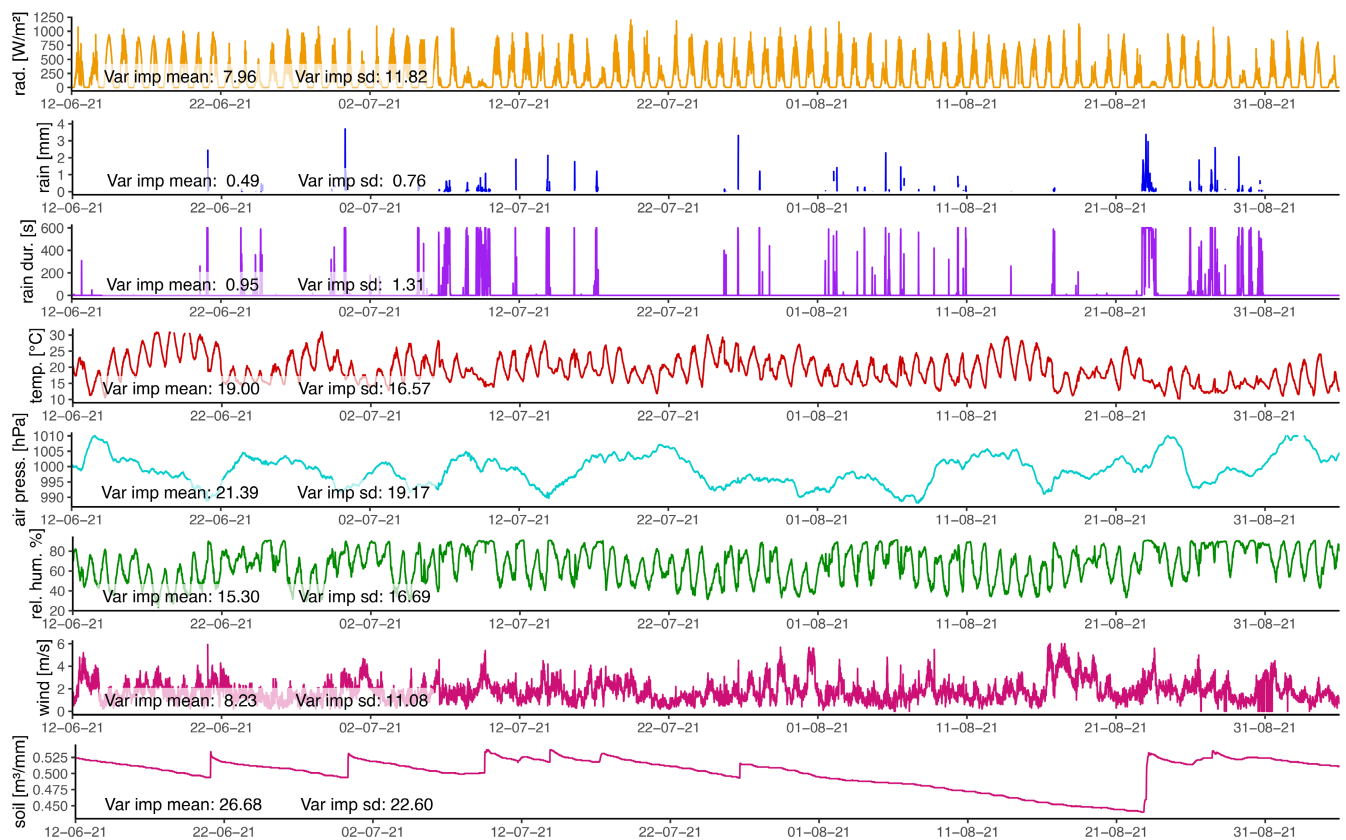
FIGURE 7 Environmental variables recorded at the top of the Leipzig Canopy Crane (LCC; 35 m height) and their relative contribution to random forest models predicting the moving average (Var imp mean) and moving standard deviation (Var imp sd) of leaf angles. Higher variable importance indicates higher contribution to the random forest model. Solar radiance (rad.), rain, rain duration (rain dur.), air temperature (temp.), air pressure (air press.), relative humidity (rel. Hum) and wind speed (wind)

also revealed considerable fluctuations of leaf angles on small time scales (even from one image frame to another). Initial conjectures were that these fluctuations are largely caused by model uncertainty or short-term illumination variations. However, visual inspections indicated that indeed wind (and resulting turbulence) drives a stochastic movement of leaves during most time periods (for an animation, see https://github.com/tejakattenborn/AngleCam), which is supported by the relatively constant winds observed (Figure 7). The generated time series was based on an interval of 3 min to constrain data volumes (to around 3 TB). The original time series was recorded at a 1-min interval, while the Brinno-TLC200 Pro can be set to intervals of seconds to hours. Depending on the field of application, small intervals are to be preferred since they facilitate to either track or at least compensate such short-term variations.

It is important to consider that the AngleCam method is not intended and not necessarily capable of predicting the leaf angle distribution of an entire canopy of a plant individual. The successful evaluation of AngleCam with TLSLeAF outputs, with the latter representing whole canopies, suggests that the predictions can indeed be representative of an entire plant canopy (Figure 4). This was possible as the plants sizes in this experiment enabled to image most of their canopies in a single frame and as we acquired multiple images from different perspectives. However, the CNN model was trained

with leaf angle distributions sampled from each individual image (not from the whole plant individual), meaning that the model will predict the leaf angle distribution for the canopy section shown in the imagery (*what you see is what you get*). We do not view this as a limitation but as opportunity for assessing the heterogeneity of plant environment relationships within canopies.

The temporal variation in leaf angles greatly differed between *A. pseudoplatanus* and *T. cordata* as expected for functionally different species (Geldhof et al., 2021). We also observed considerable departures of individual time series obtained with camera positions at top and within crowns of the assessed tree individuals. Overall, time series obtained within canopies showed a higher agreement, which may be attributed to more homogeneous environmental conditions within a forest stand. In contrast, an increased atmospheric coupling and heterogeneous exposition to solar radiance at the top of canopies may explain why the corresponding time series show a weaker correspondence. Yet, the leaf angle time series derived from all camera positions could be accurately predicted from environmental drivers using random forest models, further underlining the plausibility of each individual time series.

For both species, leaf angles were generally higher at the crown tops than within crowns. This agrees with previous findings (e.g.
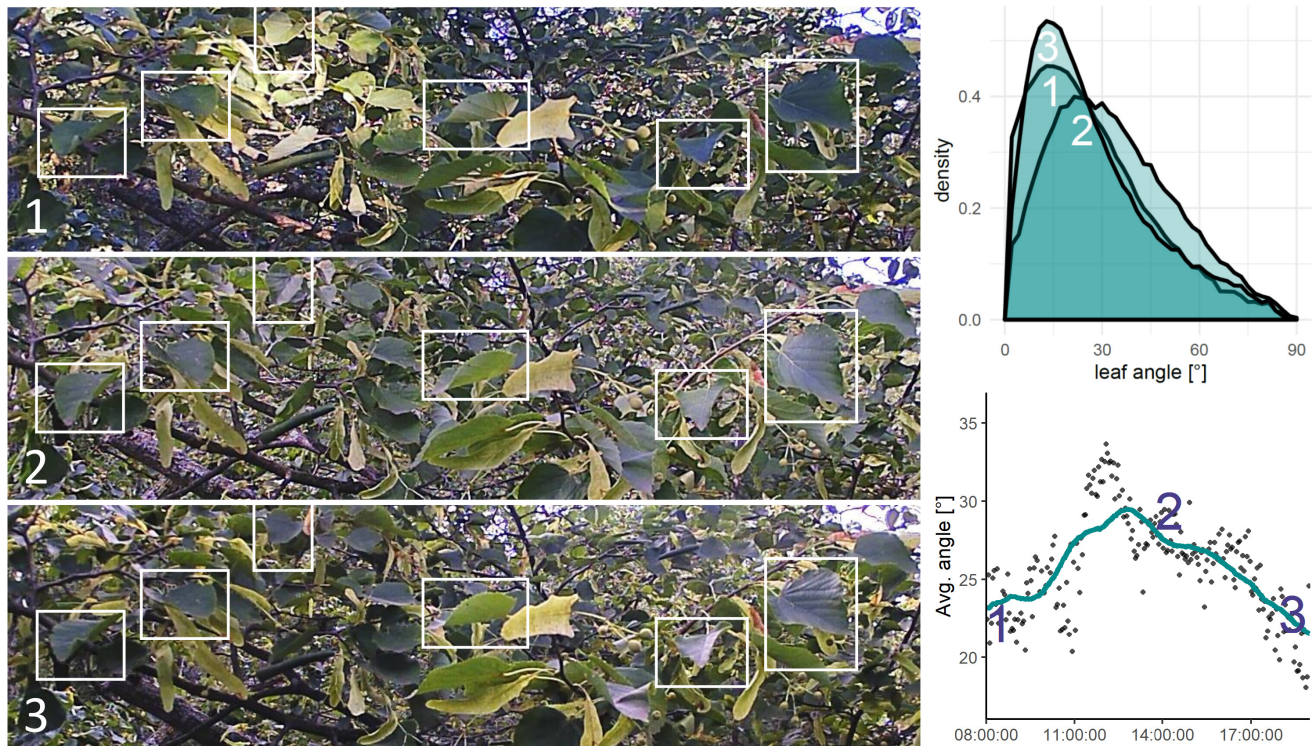
FIGURE 8 Three sample images within a crown of *Tilia cordata* (left) along the course of a day (13 August 2021). The white boxes were added to ease the comparison of vertical leave movements through time. The model predictions are illustrated by the corresponding leaf angle distribution (top right) and the average leaf angles of these samples along the predicted time series (bottom right). The cyan line shows the moving mean of the average leaf angle. For visualization, the original imagery was cropped (40% horizontally and 60% vertically). An animation with all individual image frames is given in the GitHub-repository (https://github.com/tejakattenborn/AngleCam).

Stovall et al., 2021) and highlights that the variation of leaf angles at multiple height layers has to be assessed for a full understanding of leaf angle variation in plant canopies (Niinemets, 2010). In this regard, low-cost cameras as used in the present study can provide an effective method to understand the variation of plant morphological responses across a plant's canopy. In contrast, specific applications may require specific and comparable camera positions. For instance, leaf angles as an indicator for plant stress are expected to be more sensitive to heat, water and radiation stress at the outer perimeter or top of a tree crown, where hydraulic resistance and the variation of stomatal conductance are commonly most pronounced (Grote et al., 2016).

Overall, the time series underlined that leaf angles are not a static quantity but vary considerably on multiple time scales. In many research and application areas, leaf angles distributions are assumed to be constant, including plant growth modelling (Guo et al., 2011), Earth system modelling (Rogers et al., 2017) or radiative transfer modelling and remote sensing (Berger et al., 2018; Kattenborn et al., 2018). However, the influence of this temporal variation can be critical, for instance on scattering properties of plant canopies. The temporal variation of leaf angles for *A. pseudoplatanus* and *T. cordata* was expected to alter the mean reflectance from 400 to 2500 nm up to 11% and 22%, respectively (see Appendix for details how these estimates were derived using the radiative transfer model PROSAIL-5b). Such variation greatly impact a plant's energy budget

(Sastry et al., 2018) and constrains, if not accounted for, the retrieval of plant properties with Earth observation signals (Braghiere et al., 2021; Dechant et al., 2020; Hase et al., 2022). Note that the weather in 2021 at the LCC site was characterized by frequent rain events and the absence of droughts and extreme temperatures (Figure 7), meaning that the time series did not even resemble the full spectrum of potential leaf angles.

The relationship of leaf angles with environmental drivers was unexpectedly strong. Yet, these correlations do not necessarily imply that all short-term variations in leaf angles can be implicitly explained by short-term environmental effects. It is likely that a considerable oscillation in leaf angles are hard-coded nastic movements and follow the circadian rhythm, which, in turn, can be synchronized with the prevailing oscillations of several environmental drivers (Geldhof et al., 2021; Greenham & McClung, 2015; McClung, 2006), such as solar radiation, temperature or relative humidity (Figure 7). The random forest variable importance suggests that most of the included environmental variables had a considerable effect on predicting leaf angles (Figure 7). Largest effects (importance) were observed for variables that are main determinants of transpiration, that is, soil humidity, temperature, air pressure and relative humidity (Grantz, 1990; Zhu et al., 2022). Yet, visual inspection of the imagery revealed abrupt changes in leaf angles during rain events, most likely due to additional weight of adhering rain droplets, that are well reflected by the predicted leaf

angles (Figure 7). This may not be reflected in the variable importance of rain, as such events are only relevant for short periods of time. Also note that the variable importance represents statistical and not causal relationships and that the models may indirectly account for the effect of rain through variables that are highly correlated during such events, such as solar radiance, relative humidity or temperature (Figure 7).

4.3 | General considerations and outlook

In addition to the successful evaluation of AngleCam, the experiment conducted at the LCC site highlighted that the proposed software and hardware are operational under field conditions. The cameras were installed from end of May to end of September and were exposed to adverse environmental conditions, including direct and intense solar radiation, large variability of temperature and humidity (Figure 7) and multiple storms with peak wind speeds measured above 20m/s (not shown). The cameras used also do not need an external power supply and due to the long run-time and robustness of the Brinno TLC200 Pro, the installation and maintenance effort is low.

AngleCam proved to be very efficient in terms data acquisition and analysis. The sensor installation is straightforward and only requires a fixed position with horizontal orientation (here visually estimated) and a distance in which the shape of individual leaves can be recognized (depending on leaf size). The maintenance of the cameras during the entire duration of the experiment was restricted to only two dates (Figure 6). In contrast to previously published methods based on TLS (Stovall et al., 2021), consumer-grade cameras with visual interpretation (Pisek et al., 2011; Ryu et al., 2010), stereo imaging (Bernotas et al., 2019; Müller-Linow et al., 2015) or segmentation approaches (Raju et al., 2020), the AngleCam method does not require manual input, sensor calibration, data pre-processing or sophisticated data acquisition procedures and can readily applied in field conditions.

All imagery in this study was recorded using the Brinno TLC200 Pro. The applicability of the models on imagery acquired by other cameras was not explicitly tested. We assume that the models are transferable as long as lens characteristics do not strongly deviate. It can be assumed that the model is transferable across different scene conditions, since the model was trained on a very heterogeneous image dataset, including variation in camera–plant distance, backgrounds, outdoor and indoor settings, illumination conditions, or presence of artificial objects. Note that the openly available model objects can be updated with additional data, enabling to enlarge the area of applicability in terms of cameras, plant species and application scenarios. Until now, the models are primarily trained for broadleaf plants. Upcoming versions will also be optimized for needle-leaved and grass species.

The current approach is based on horizontal camera orientations, where, depending on the horizontal field of view in an image, leaves are primarily viewed from the side. As the leaf angle describes the inclination of the leaf surface on a vertical axis, this *side view* is assumed to be most robust (Pisek et al., 2011). We did not test to what extend the presented model is applicable to a non-horizontal perspective or whether they may have to be trained on such data.

The basis for the CNN model was the EfficientNet-B7 as backbone (Tan & Le, 2019), which was found most accurate and efficient compared to common available backbones (we also tested variants of other backbone families, including ResNet, MobileNet, DenseNet). Training the EfficientNet-B7-based model in 200 epochs took about 2h using a NVIDIA A6000. The time to predict the leaf angle distribution for the entirely image time series of all cameras (317,348 images) took less than 30min. Upcoming research may include the use or integration of newer backbones or even ensemble versions (Schiller et al., 2021).

The output of AngleCam (leaf angle distributions or derivatives) can be directly integrated into various applications, including functional-structural plant modelling to assess production and ecophysiology in crops or ecosystems (Louarn & Song, 2020; Vos et al., 2010), Earth system modelling to reveal ecosystem fluxes and processes (Bonan et al., 2014; Heidkamp et al., 2020; Rogers et al., 2017), radiative transfer modelling and remote sensing, where, despite the cardinal importance of leaf angles for scattering processes (Dechant et al., 2020; Hase et al., 2022), leaf angle observations remain sparse (Berger et al., 2018). Such leaf angle estimates may also facilitate modelling of plant competition and community composition (Charbonnier et al., 2013; Falster & Westoby, 2003; Van Zanten et al., 2010). In the context of the increased intensities and frequencies of climate extremes impacting agriculture, forestry and ecosystems (Betts et al., 2018; Lange et al., 2020), AngleCam may be applicable to track responses resulting from heat, water or radiation stress. Extending the camera system used here with Wifi-compatible SD cards or using other camera models could enable to establish sensor networks for real-time monitoring of stress responses or vitality status, respectively.

The presented approach is particularly designed to track nastic movements, that is, non-directional leaf movements along the vertical axis. Plants can also perform tropic movements and change their directional leaf orientation towards a stimuli (Hart, 1990). An example are paraheliotropic movements, which turn leaf surfaces perpendicular to sun rays to avoid excess radiation or reduce leaf temperatures. The presented approach may be extended to track such tropic movements with corresponding training data and taking the azimuth angle of the camera orientation into account. Moreover, AngleCam may be extended to explicitly quantify the degree of general leaf stress symptoms, such as drooping, wilting or rolling (Sastry et al., 2018). Yet, such stress responses may be very species-specific. For instance, during the drought events in 2018 at the LCC *T. cordata* was observed to invert its leaves during heat stress with the bright bottom side facing upwards reducing the albedo (the same response was reported for *Tilia comentosa* in Hirons & Thomas, 2018).

AngleCam may not only be used to track leaf angle through time, but also predict leaf angles for individual images. This could, for instance, be used to efficiently feed leaf angle observations to trait databases such as TRY (Kattge et al., 2020), which are extremely sparse in this context. Such potentials may be even accelerated with the

concurrent developments of big data in ecology (Depauw et al., 2022; Farley et al., 2018). Data gaps of leaf angles across species may be filled with AngleCam and in concert with the ever increasing availability of citizen science photographs and species labels (the iNaturalist project, Di Cecco et al., 2021; Schiller et al., 2021). Likewise, AngleCam may be applicable to data streams from PhenoCam networks (Aasen et al., 2020; Seyednasrollah et al., 2019) to track plant phenology and its relationship with environmental drivers across the globe.

5 | CONCLUSIONS

Vertical leaf angles and their variation through time are directly related to several ecophysiological processes and properties and are thus a cardinal for several applications in the context of plant and ecosystem productivity, stress responses to extreme events and Earth observation. While effective methods to track leaf angles remain sparse, we present AngleCam, a method to estimate leaf angles from horizontal plant photographs using CNNs and low-cost outdoor cameras. The performance of AngleCam was successfully tested across species and growth forms with reference data of independent samples as well as leaf angle estimates derived from TLS. The AngleCam method in concert with consumer-grade outdoor cameras was tested for generating long-term and high-resolution time series under field conditions (3-min interval, 4-month observation period). The predicted temporal variation in leaf angles could be accurately explained with environmental drivers, further underlining the plausibility and relevance of the method. The output of AngleCam and potential derivatives are directly compatible with a range of applications, including functional-structural plant modelling, Earth system modelling or radiative transfer modelling.

AUTHOR CONTRIBUTIONS

Teja Kattenborn and Ronny Richter conceived the ideas and designed the methodology; Teja Kattenborn, Ronny Richter, Claudia Guimarães-Steinicke collected the data; Teja Kattenborn analysed the data; Teja Kattenborn led the writing of the manuscript. All authors contributed critically to the drafts and gave final approval for publication.

CONFLICTS OF INTEREST

All authors declare that they have no conflicts of interest.

PEER REVIEW

The peer review history for this article is available at https://publons.com/publon/10.1111/2041-210X.13968.

ORCID

Teja Kattenborn https://orcid.org/0000-0001-7381-3828
Ronny Richter https://orcid.org/0000-0002-8728-7918
Claudia Guimarães-Steinicke https://orcid.org/0000-0001-7829-641X
Hannes Feilhauer https://orcid.org/0000-0001-5758-6303
Christian Wirth https://orcid.org/0000-0003-2604-8056

REFERENCES

Aasen, H., Kirchgessner, N., Walter, A., & Liebisch, F. (2020). Phenocams for field phenotyping: Using very high temporal resolution digital repeated photography to investigate interactions of growth, phenology, and harvest traits. *Frontiers in Plant Science*, 11, 593.

Albawi, S., Mohammed, T. A., & Al-Zawi, S. (2017). Understanding of a convolutional neural network. *2017 International Conference on Engineering and Technology (ICET)*, 1–6.

Apelt, F., Breuer, D., Olas, J. J., Annunziata, M. G., Flis, A., Nikoloski, Z., Kragler, F., & Stitt, M. (2017). Circadian, carbon, and light control of expansion growth and leaf movement. *Plant Physiology*, 174(3), 1949–1968.

Bailey, B. N., & Mahaffee, W. F. (2017). Rapid measurement of the three-dimensional distribution of leaf orientation and the leaf angle probability density function using terrestrial lidar scanning. *Remote Sensing of Environment*, 194, 63–76.

Berger, K., Atzberger, C., Danner, M., D'Urso, G., Mauser, W., Vuolo, F., & Hank, T. (2018). Evaluation of the prosail model capabilities for future hyperspectral model environments: A review study. *Remote Sensing*, 10(1), 85.

Bernotas, G., Scorza, L. C., Hansen, M. F., Hales, I. J., Halliday, K. J., Smith, L. N., Smith, M. L., & McCormick, A. J. (2019). A photometric stereo-based 3D imaging system using computer vision and deep learning for tracking plant growth. *GigaScience*, 8(5), giz056.

Betts, R. A., Alfieri, L., Bradshaw, C., Caesar, J., Feyen, L., Friedlingstein, P., Gohar, L., Koutroulis, A., Lewis, K., Morfopoulos, C., Papadimitriou, L., Richardson, K. J., Tsanis, I., & Wyser, K. (2018). Changes in climate extremes, fresh water availability and vulnerability to food insecurity projected at 1.5°C and 2°C global warming with a higher-resolution global climate model. *Philosophical Transactions of the Royal Society A: Mathematical, Physical and Engineering Sciences*, 376(2119), 20160452.

Biskup, B., Scharr, H., Schurr, U., & Rascher, U. (2007). A stereo imaging system for measuring structural parameters of plant canopies. *Plant, Cell & Environment*, 30(10), 1299–1308.

Bonan, G., Williams, M., Fisher, R., & Oleson, K. (2014). Modeling stomatal conductance in the earth system: Linking leaf water-use efficiency and water transport along the soil–plant–atmosphere continuum. *Geoscientific Model Development*, 7(5), 2193–2222.

Braghiere, R. K., Wang, Y., Doughty, R., Sousa, D., Magney, T., Widlowski, J.-L., Longo, M., Bloom, A. A., Worden, J., Gentine, P., & Frankenberg, C. (2021). Accounting for canopy structure improves hyperspectral radiative transfer and sun-induced chlorophyll fluorescence representations in a new generation earth system model. *Remote Sensing of Environment*, *261*, 112497.

Breiman, L. (2001). Random forests. *Machine Learning*, *45*(1), 5–32.

Cao, M., & Xin, Q. (2021). A deep learning method for detecting leaf phenology from phenocam imagery. *2021 IEEE International Geoscience and Remote Sensing Symposium (IGARSS)*, 6889–6892.

Charbonnier, F., Le Maire, G., Dreyer, E., Casanoves, F., Christina, M., Dauzat, J., Eitel, J. U., Vaast, P., Vierling, L. A., & Roupsard, O. (2013). Competition for light in heterogeneous canopies: Application of maestra to a coffee (*Coffea arabica* L.) agroforestry system. *Agricultural and Forest Meteorology*, *181*, 152–169.

CloudCompare. (2022). *Cloudcompare 2.12. beta*.

Correia, D. L., Bouachir, W., Gervais, D., Pureswaran, D., Kneeshaw, D. D., & De Grandpré, L. (2020). Leveraging artificial intelligence for large-scale plant phenology studies from noisy time-lapse images. *IEEE Access*, *8*, 13151–13160.

Darwin, C., & Darwin, F. (1880). *The power of movement in plants*. John Murray.

Debeer, D., Hothorn, T., Strobl, C., & Debeer, M. D. (2021). *Package 'permimp'*.

Dechant, B., Ryu, Y., Badgley, G., Zeng, Y., Berry, J. A., Zhang, Y., Goulas, Y., Li, Z., Zhang, Q., Kang, M., Li, J., & Moya, I. (2020). Canopy structure explains the relationship between photosynthesis and sun-induced chlorophyll fluorescence in crops. *Remote Sensing of Environment*, *241*, 111733.

Depauw, L., Blondeel, H., De Lombaerde, E., De Pauw, K., Landuyt, D., Lorer, E., Vangansbeke, P., Vanneste, T., Verheyen, K., & De Frenne, P. (2022). The use of photos to investigate ecological change. *Journal of Ecology*, *110*, 1220–1236.

Di Cecco, G. J., Barve, V., Belitz, M. W., Stucky, B. J., Guralnick, R. P., & Hurlbert, A. H. (2021). Observing the observers: How participants contribute data to inaturalist and implications for biodiversity science. *Bioscience*, *71*(11), 1179–1188.

Ehleringer, J., & Comstock, J. (1987). Leaf absorptance and leaf angle: Mechanisms for stress avoidance. In *Plant response to stress* (pp. 55–76). Springer.

Falster, D. S., & Westoby, M. (2003). Plant height and evolutionary games. *Trends in Ecology & Evolution*, *18*(7), 337–343.

Farley, S. S., Dawson, A., Goring, S. J., & Williams, J. W. (2018). Situating ecology as a big-data science: Current advances, challenges, and solutions. *Bioscience*, *68*(8), 563–576.

Geldhof, B., Pattyn, J., Eyland, D., Carpentier, S., & Van de Poel, B. (2021). A digital sensor to measure real-time leaf movements and detect abiotic stress in plants. *Plant Physiology*, *187*(3), 1131–1148.

Goel, N. S., & Strebel, D. E. (1984). Simple beta distribution representation of leaf orientation in vegetation canopies 1. *Agronomy Journal*, *76*(5), 800–802.

Grantz, D. (1990). Plant response to atmospheric humidity. *Plant, Cell & Environment*, *13*(7), 667–679.

Greenham, K., & McClung, C. R. (2015). Integrating circadian dynamics with physiological processes in plants. *Nature Reviews Genetics*, *16*(10), 598–610.

Grote, R., Gessler, A., Hommel, R., Poschenrieder, W., & Priesack, E. (2016). Importance of tree height and social position for drought-related stress on tree growth and mortality. *Trees*, *30*(5), 1467–1482.

Guo, Y., Fourcaud, T., Jaeger, M., Zhang, X., & Li, B. (2011). Plant growth and architectural modelling and its applications. *Annals of Botany*, *107*(5), 723–727.

Hart, J. W. (1990). *Plant tropisms: And other growth movements*. Springer Science & Business Media.

Hase, N., Doktor, D., Rebmann, C., Dechant, B., Mollenhauer, H., & Cuntz, M. (2022). Identifying the main drivers of the seasonal decline of near-infrared reflectance of a temperate deciduous forest. *Agricultural and Forest Meteorology*, *313*, 108746.

Heidkamp, M., Ament, F., de Vrese, P., & Chlond, A. (2020). Studying the large-scale effect of leaf thermoregulation using an earth system model. *Earth System Dynamics Discussions*, 1–28 [preprint].

Hikosaka, K., & Hirose, T. (1997). Leaf angle as a strategy for light competition: Optimal and evolutionary stable light-extinction coefficient within a leaf canopy. *Ecoscience*, *4*(4), 501–507.

Hirons, A., & Thomas, P. A. (2018). *Applied tree biology*. John Wiley & Sons.

Hoeser, T., & Kuenzer, C. (2020). Object detection and image segmentation with deep learning on earth observation data: A review-part i: Evolution and recent trends. *Remote Sensing*, *12*(10), 1667.

Itakura, K., & Hosoi, F. (2019). Estimation of leaf inclination angle in three-dimensional plant images obtained from lidar. *Remote Sensing*, *11*(3), 344.

Jacquemoud, S., Verhoef, W., Baret, F., Bacour, C., Zarco-Tejada, P. J., Asner, G. P., François, C., & Ustin, S. L. (2009). Prospect+ sail models: A review of use for vegetation characterization. *Remote Sensing of Environment*, *113*, S56–S66.

Kattenborn, T., Eichel, J., & Fassnacht, F. E. (2019). Convolutional neural networks enable efficient, accurate and fine-grained segmentation of plant species and communities from high-resolution UAV imagery. *Scientific Reports*, *9*(1), 17656. https://doi.org/10.1038/s41598-019-53797-9

Kattenborn, T., Fassnacht, F. E., & Schmidtlein, S. (2018). Differentiating plant functional types using reflectance: Which traits make the difference? *Remote Sensing in Ecology and Conservation*, *5*(1), 5–19. https://doi.org/10.1002/rse2.86

Kattenborn, T., Leitloff, J., Schiefer, F., & Hinz, S. (2021). Review on convolutional neural networks (CNN) in vegetation remote sensing. *ISPRS Journal of Photogrammetry and Remote Sensing*, *173*(2020), 24–49. https://doi.org/10.1016/j.isprsjprs.2020.12.010

Kattenborn, T., Ronny, R., Claudia, G.-S., Feilhauer, H., & Wirth, C. (2022a). *Anglecam* (Version 2022-04-07). https://doi.org/10.5281/zenodo.6812108

Kattenborn, T., Ronny, R., Claudia, G.-S., Feilhauer, H., & Wirth, C. (2022b). *Anglecam publication data (methods in ecology and evolution, MEE)*. https://doi.org/10.5281/zenodo.6929177

Kattge, J., Bönisch, G., Diaz, S., Lavorel, S., Prentice, I. C., Leadley, P., Tautenhahn, S., Werner, G. D., Aakala, T., Abedi, M., Acosta, A. T. R., Adamidis, G. C., Adamson, K., Aiba, M., Albert, C. H., Alcántara, J. M., Carolina Alcázar, C., Aleixo, I., Ali, H., ... Wirth, C. (2020). Try plant trait database–enhanced coverage and open access. *Global Change Biology*, *26*(1), 119–188.

Kim, S., & Burge, J. (2020). Natural scene statistics predict how humans pool information across space in surface tilt estimation. *PLoS Computational Biology*, *16*(6), e1007947.

Lange, S., Volkholz, J., Geiger, T., Zhao, F., Vega, I., Veldkamp, T., Reyer, C. P., Warszawski, L., Huber, V., Jägermeyr, J., Schewe, J., Bresch, D. N., Büchner, M., Chang, J., Ciais, P., Dury, M., Emanuel, K., Folberth, C., Gerten, D., ... Frieler, K. (2020). Projecting exposure to extreme climate impact events across six event categories and three spatial scales. *Earth's Futures*, *8*(12), e2020EF001616.

Leuzinger, S., & Körner, C. (2007). Tree species diversity affects canopy leaf temperatures in a mature temperate forest. *Agricultural and Forest Meteorology*, *146*(1–2), 29–37.

Louarn, G., & Song, Y. (2020). Two decades of functional–structural plant modelling: Now addressing fundamental questions in systems biology and predictive ecology. *Annals of Botany*, *126*(4), 501–509.

Mantilla-Perez, M. B., & Salas Fernandez, M. G. (2017). Differential manipulation of leaf angle throughout the canopy: Current status and prospects. *Journal of Experimental Botany*, *68*(21–22), 5699–5717.

McClung, C. R. (2006). Plant circadian rhythms. *The Plant Cell*, *18*(4), 792–803.

Mohanty, S. P., Hughes, D. P., & Salathé, M. (2016). Using deep learning for image-based plant disease detection. *Frontiers in Plant Science*, *7*, 1419.

Moorthy, S. M. K., Calders, K., Vicari, M. B., & Verbeeck, H. (2019). Improved supervised learning- based approach for leaf and wood classification from lidar point clouds of forests. *IEEE Transactions on Geoscience and Remote Sensing*, 58(5), 3057–3070.

Mullen, J. L., Weinig, C., & Hangarter, R. P. (2006). Shade avoidance and the regulation of leaf inclination in arabidopsis. *Plant, Cell & Environment*, 29(6), 1099–1106.

Müller-Linow, M., Pinto-Espinosa, F., Scharr, H., & Rascher, U. (2015). The leaf angle distribution of natural plant populations: Assessing the canopy with a novel software tool. *Plant Methods*, 11(1), 1–16.

Niinemets, Ü. (2010). A review of light interception in plant stands from leaf to canopy in different plant functional types and in species with varying shade tolerance. *Ecological Research*, 25(4), 693–714.

Pepper, G., Pearce, R., & Mock, J. (1977). Leaf orientation and yield of maize 1. *Crop Science*, 17(6), 883–886.

Pisek, J., Ryu, Y., & Alikas, K. (2011). Estimating leaf inclination and g- function from leveled digital camera photography in broadleaf canopies. *Trees*, 25(5), 919–924.

Puglielli, G., Redondo-Gómez, S., Gratani, L., & Mateos-Naranjo, E. (2017). Highlighting the differential role of leaf paraheliotropism in two mediterranean cistus species under drought stress and well- watered conditions. *Journal of Plant Physiology*, 213, 199–208.

Qi, J., Xie, D., Li, L., Zhang, W., Mu, X., & Yan, G. (2019). Estimating leaf angle distribution from smartphone photographs. *IEEE Geoscience and Remote Sensing Letters*, 16(8), 1190–1194.

R Core Team. (2013). *R: A language and environment for statistical computing*. R Foundation for Statistical Computing.

Raju, S. K. K., Adkins, M., Enersen, A., Santana de Carvalho, D., Studer, A. J., Ganapathysubramanian, B., Schnable, P. S., & Schnable, J. C. (2020). Leaf angle extractor: A high-throughput image processing framework for leaf angle measurements in maize and sorghum. *Applications in Plant Sciences*, 8(8), e11385.

Richter, R., Ballasus, H., Engelmann, R. A., Zielhofer, C., & Wirth, C. (2022). Tree species matter for forest microclimate regulation during the drought year 2018: Disentangling environmental drivers and biotic drivers. *Nature Scientific Reports* [preprint].

Richter, R., Hutengs, C., Wirth, C., Bannehr, L., & Vohland, M. (2021). Detecting tree species effects on forest canopy temperatures with thermal remote sensing: The role of spatial resolution. *Remote Sensing*, 13(1), 135.

Rogers, A., Medlyn, B. E., Dukes, J. S., Bonan, G., Von Caemmerer, S., Dietze, M. C., Kattge, J., Leakey, A. D., Mercado, L. M., Niinemets, Ü., Prentice, I. C., Serbin, S. P., Sitch, S., Way, D. A., & Zaehle, S. (2017). A roadmap for improving the representation of photosynthesis in earth system models. *New Phytologist*, 213(1), 22–42.

Rolnick, D., Veit, A., Belongie, S., & Shavit, N. (2017). Deep learning is robust to massive label noise. *arXiv preprint arXiv:1705.10694*.

Ryu, Y., Sonnentag, O., Nilson, T., Vargas, R., Kobayashi, H., Wenk, R., & Baldocchi, D. D. (2010). How to quantify tree leaf area index in an open savanna ecosystem: A multi-instrument and multi-model approach. *Agricultural and Forest Meteorology*, 150(1), 63–76.

Sarlikioti, V., De Visser, P., & Marcelis, L. (2011). Exploring the spatial distribution of light interception and photosynthesis of canopies by means of a functional–structural plant model. *Annals of Botany*, 107(5), 875–883.

Sastry, A., Guha, A., & Barua, D. (2018). Leaf thermotolerance in dry tropical forest tree species: Relationships with leaf traits and effects of drought. *AoB Plants*, 10(1), plx070.

Schiefer, F., Kattenborn, T., Frick, A., Frey, J., Schall, P., Koch, B., & Schmidtlein, S. (2020). Mapping forest tree species in high resolution UAV-based RGB-imagery by means of convolutional neural networks. *ISPRS Journal of Photogrammetry and Remote Sensing*, 170(January), 205–215. https://doi.org/10.1016/j.isprsjprs.2020.10.015

Schiller, C., Schmidtlein, S., Boonman, C., Moreno-Martínez, A., & Kattenborn, T. (2021). Deep learning and citizen science enable automated plant trait predictions from photographs. *Scientific Reports*, 11(1), 1–12.

Seyednasrollah, B., Young, A. M., Hufkens, K., Milliman, T., Friedl, M. A., Frolking, S., & Richardson, A. D. (2019). Tracking vegetation phenology across diverse biomes using version 2.0 of the phenocam dataset. *Scientific Data*, 6(1), 1–11.

Singh, A. K., Ganapathysubramanian, B., Sarkar, S., & Singh, A. (2018). Deep learning for plant stress phenotyping: Trends and future perspectives. *Trends in Plant Science*, 23(10), 883–898.

Spelke, E., Lee, S. A., & Izard, V. (2010). Beyond core knowledge: Natural geometry. *Cognitive Science*, 34(5), 863–884.

Stovall, A. E., Masters, B., Fatoyinbo, L., & Yang, X. (2021). Tlsleaf: Automatic leaf angle estimates from single-scan terrestrial laser scanning. *New Phytologist*, 232(4), 1876–1892.

Strobl, C., Boulesteix, A.-L., Kneib, T., Augustin, T., & Zeileis, A. (2008). Conditional variable importance for random forests. *BMC Bioinformatics*, 9(1), 1–11.

Tan, M., & Le, Q. (2019). Efficientnet: Rethinking model scaling for convolutional neural networks. *International conference on machine learning*, 6105–6114.

Van Zanten, M., Pons, T., Janssen, J., Voesenek, L., & Peeters, A. (2010). On the relevance and control of leaf angle. *Critical Reviews in Plant Science*, 29(5), 300–316.

Vicari, M. B., Pisek, J., & Disney, M. (2019). New estimates of leaf angle distribution from terrestrial lidar: Comparison with measured and modelled estimates from nine broadleaf tree species. *Agricultural and Forest Meteorology*, 264, 322–333.

Vos, J., Evers, J. B., Buck-Sorlin, G. H., Andrieu, B., Chelle, M., & De Visser, P. H. (2010). Functional–structural plant modelling: A new versatile tool in crop science. *Journal of Experimental Botany*, 61(8), 2101–2115.

Wang, W., Li, Z., & Su, H. (2007). Comparison of leaf angle distribution functions: Effects on extinction coefficient and fraction of sunlit foliage. *Agricultural and Forest Meteorology*, 143(1–2), 106–122.

Xu, S., Atherton, J., Riikonen, A., Zhang, C., Oivukkamäki, J., MacArthur, A., Honkavaara, E., Hakala, T., Koivumäki, N., Liu, Z., & Porcar-Castell, A. (2021). Structural and photosynthetic dynamics mediate the response of sif to water stress in a potato crop. *Remote Sensing of Environment*, 263, 112555.

Zhu, Y., Cheng, Z., Feng, K., Chen, Z., Cao, C., Huang, J., Ye, H., & Gao, Y. (2022). Influencing factors for transpiration rate: A numerical simulation of an individual leaf system. *Thermal Science and Engineering Progress*, 27, 101110.

Zou, X., Möttus, M., Tammeorg, P., Torres, C. L., Takala, T., Pisek, J., Mäkelä, P., Stoddard, F., & Pellikka, P. (2014). Photographic measurement of leaf angles in field crops. *Agricultural and Forest Meteorology*, 184, 137–146.

SUPPORTING INFORMATION

Additional supporting information can be found online in the Supporting Information section at the end of this article.